Analysis Method for Generalized Suspended Striplines

EIKICHI YAMASHITA, FELLOW, IEEE, MASAYUKI NAKAJIMA, AND KAZUHIKO ATSUKI

Abstract—**This paper describes an effective analysis method suited to generalized suspended striplines, that is, planar transmission lines having multiple conductor sheets on multiple substrates, and multiple supporting grooves or pedestals. Two example striplines structures are analyzed based on this method. Some experimental results are also shown.**

I. Introduction

SUSPENDED STRIPLINES (SSL's) have recently been used in many areas such as planar filter structures [1] and millimeter-wave devices [2] by taking advantage of their ease of fabrication and low lossness. SSL's also have a possibility to be used to compose part of monolithic microwave integrated circuits.

This paper first defines a class of striplines and an original analysis method particularly suited to characterize this class of striplines. Then, two example coupled stripline structures having a conductor aperture between two strips are analyzed based on this method. The results of the analysis are compared with experimental data in the form of capacitance matrix elements.

This semianalytic method has the merit of small matrix dimensions compared with the finite-difference method, the finite-element method, or the boundary-element method.

II. Generalized Suspended Striplines

Fig. 1(a) shows the cross-sectional view of a class of striplines, that is, generalized suspended striplines (GSSL's). The cross section is composed of several homogeneous square regions with two opposed conductor walls; the regions are located in parallel and are connected with each other with common boundaries. Each of these regions can be filled with either substrate material or air. The boundary surface between two adjacent regions may be covered partly with a strip conductor or an extended ground conductor. The substrates of these structures can be suspended by grooves or pedestals. A variety of new stripline structures, as shown in Fig. 1(b), can be conceived by applying GSSL's.

III. Analysis Procedure

We seek the capacitance matrix as the basic parameters of GSSL's by assuming low loss and weak dispersion in the transmission of the fundamental mode and by extending the analysis method given in a previous paper [3].

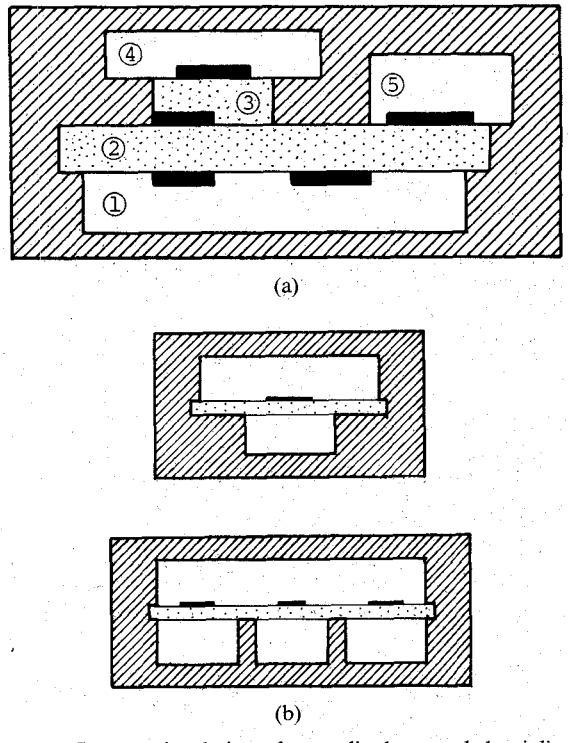

Fig. 1. (a) Cross-sectional view of generalized suspended striplines. (b) Other examples of GSSL's.

Laplace's equation is the basic equation to be solved in the quasi-TEM wave analysis of GSSL's. An outline of the analysis steps follows.

1) Specify the potential at each conductor.

2) Expand the potential $\phi_i(x_i, y_i)$ defined in the region i in the Fourier series form as

$$\phi_i(x_i, y_i) = \sum_{n=1}^{\infty} \left[A_{ni} \sinh\left(\frac{n\pi y_i}{a_i}\right) + B_{ni} \cosh\left(\frac{n\pi y_i}{a_i}\right) \right] \sin\left(\frac{n\pi x_i}{a_i}\right) \quad (1)$$

where a_i is the width of region i and the origin of the x_i-axis is taken at the left end of each region. This potential form satisfies Laplace's equation within each region and a boundary condition at two opposed conductor surfaces.

Manuscript received March 4, 1986; revised June 23, 1986.

The authors are with the University of Electro-Communications, Chofu-shi, Tokyo, Japan 182.

IEEE Log Number 8610826.

3) Express the potential at each interface with the first-order spline function. The shape of the spline function determines the coefficients of the above Fourier series.

4) Express the total static field energy of this system by

$$W = \frac{1}{2}\sum_{i=1}^{N}\iint \epsilon_i \left[\left(\frac{\partial \phi_i}{\partial x}\right)^2 + \left(\frac{\partial \phi_i}{\partial y}\right)^2\right] dx_i\, dy_i. \qquad (2)$$

5) Minimize W by selecting the form of the spline functions as trial functions. A set of linear simultaneous equations is then obtained whose solutions determine potential solutions and the minimum energy $W_{\min}$.

6) The capacitance between the two conductors is then related to the minimum energy $W_{\min}$. All element values of the capacitance matrix can be obtained by the same procedure.

The merits of this method are as follows.

1) The element values of the capacitance matrix can be easily defined by initially specifying each conductor potential which is also part of the trial functions. The initial specification of conductor potentials is convenient in analyzing multiconductor systems.

2) One of the two boundary conditions, the continuity of potentials, is automatically satisfied since the surface potentials are common to two adjacent regions.

3) The other boundary condition, the continuity of the normal electric flux, is satisfied by taking the minimum of the total energy. Avoiding the imposition of explicit boundary conditions makes the present method easier than the Green's function method.

4) Since capacitance values are calculated based on the minimum-energy principle or variational principle [4], the trial functions can be expressed in a relatively simple form to reach accurate capacitance values.

5) The spline function is more adaptable to various types of surface potentials than linear combinations of continuous functions. The procedure for minimizing the energy by selecting a small number of spline knot potentials is simpler than that of directly selecting a large number of Fourier coefficients.

6) The method is simple for complicated structures. All problems of GSSL's are finally attributed to a set of linear simultaneous equations.

7) The thickness of the conductor can easily be taken into account by adding just two new regions.

8) GSSL's as shown in Fig. 1 are difficult structures to be analyzed with conformal mapping or the Green's function method. Although they can be treated with a complete numerical approach, such as the finite-difference method, the finite-element method, or the boundary-element method, the dimension of the matrices needed with these methods will be larger than that with this semianalytical method. The reason is that potential functions employed in this method satisfy wave equations within each region and boundary conditions at conductor surfaces before selecting a small number of spline knots for numerical processing.

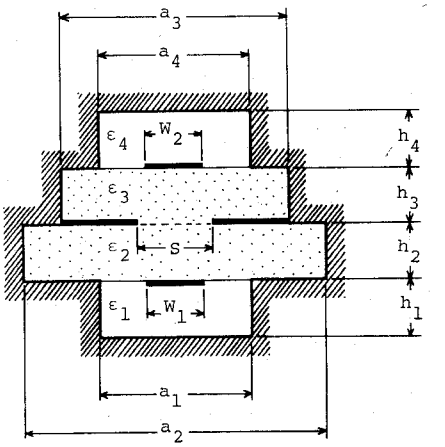

Fig. 2. An aperture coupling structure of two striplines.

IV. Aperture Coupling of Two Striplines

Fig. 2 shows an aperture coupling structure of two striplines which belongs to the category of GSSL's. The transmission characteristics of this structure are analyzed by following the above steps. The capacitance matrix in this case is defined by

$$\begin{bmatrix} Q_1 \\ Q_2 \end{bmatrix} = \begin{bmatrix} C_{11} & C_{12} \\ C_{12} & C_{22} \end{bmatrix} \begin{bmatrix} V_1 \\ V_2 \end{bmatrix} \qquad (3)$$

where Q_1 and Q_2 are the electric charge on strip conductors 1 and 2 per unit length due to given potentials V_1 and V_2 against the ground, respectively.

First, we specify $V_1 \neq 0$ and $V_2 = 0$. The potential functions of the four regions as shown in Fig. 2 are expanded as the Fourier series as

$$\phi_1(x,y) = \sum_{n=1,3,5\cdots}^{\infty} A_n \sinh\left(\frac{n\pi y}{a_1}\right)\cos\left(\frac{n\pi x}{a_1}\right), \quad \left(|x| \leqslant \frac{a_1}{2}, 0 \leqslant y \leqslant h_1\right) \qquad (4a)$$

$$\phi_2(x,y) = \sum_{n=1,3,5\cdots}^{\infty} \left[B_n \sinh\left(\frac{n\pi y}{a_2}\right) + c_n \cosh\left(\frac{n\pi y}{a_2}\right)\right]\cos\left(\frac{n\pi x}{a_2}\right), \quad \left(|x| \leqslant \frac{a_2}{2}, h_1 \leqslant y \leqslant h_1 + h_2\right) \qquad (4b)$$

$$\phi_3(x,y) = \sum_{n=1,3,5\cdots}^{\infty} \left[D_n \sinh\left(\frac{n\pi y}{a_3}\right) + E_n \cosh\left(\frac{n\pi y}{a_3}\right)\right]\cos\left(\frac{n\pi x}{a_3}\right), \quad \left(|x| \leqslant \frac{a_3}{2}, h_1 + h_2 \leqslant y \leqslant h_1 + h_2 + h_3\right) \qquad (4c)$$

$$\phi_4(x,y) = \sum_{n=1,3,5\cdots}^{\infty} F_n \sinh\left(\frac{n\pi(b-y)}{a_4}\right)\cos\left(\frac{n\pi x}{a_4}\right), \quad \left(|x| \leqslant \frac{a_4}{2}, h_1 + h_2 + h_3 \leqslant y \leqslant h_1 + h_2 + h_3 + h_4 = b\right) \qquad (4d)$$

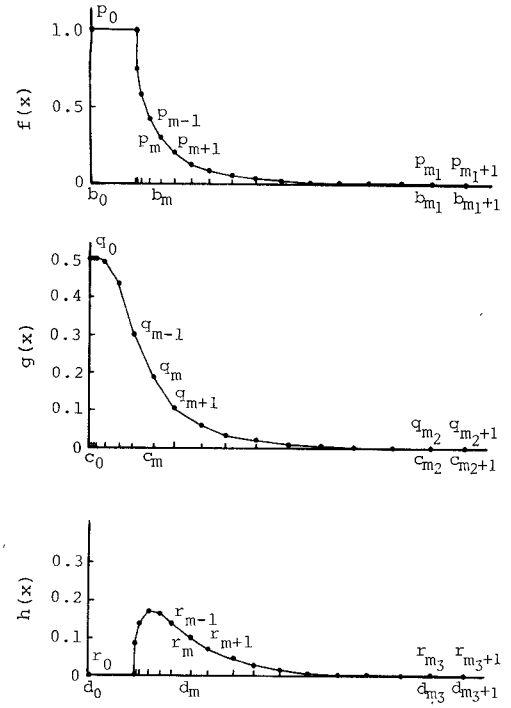

Fig. 3. Spline functions to express the three interface potentials.

where cosine functions instead of sine functions have been used because of the symmetry of this structure and the origin of the x_i-axes specified at the center.

The potential functions at each interface are defined as

$$f_1(x) = f_2(x) = f(x) \qquad \left(0 \leqslant x \leqslant \frac{a_1}{2},\ y = h_1\right) \tag{5a}$$

$$f_2(x) = 0 \qquad \left(\frac{a_1}{2} \leqslant x \leqslant \frac{a_2}{2},\ y = h_1 + 0\right) \tag{5b}$$

$$f_3(x) = f_4(x) = g(x) \qquad \left(0 \leqslant x \leqslant \frac{s}{2},\ y = h_1 + h_2\right) \tag{5c}$$

$$f_3(x) = f_4(x) = 0 \qquad \left(\frac{s}{2} \leqslant x \leqslant \frac{a_3}{2},\ y = h_1 + h_2\right) \tag{5d}$$

$$f_3(x) = 0 \qquad \left(\frac{a_3}{2} \leqslant x \leqslant \frac{a_4}{2},\ y = h_1 + h_2 - 0\right) \tag{5e}$$

$$f_5(x) = f_6(x) = h(x) \qquad \left(0 \leqslant x \leqslant \frac{a_4}{2},\ y = h_1 + h_2 + h_3\right) \tag{5f}$$

$$f_5(x) = 0 \qquad \left(\frac{a_4}{2} \leqslant x \leqslant \frac{a_3}{2},\ y = h_1 + h_2 + h_3 - 0\right). \tag{5g}$$

When the specified values of conductor potentials are considered, these interface functions are expressed with the first-order spline functions as shown in Fig. 3, where p_m, q_m, and r_m are variables to give knot potentials. These are also trial functions which are to be selected to minimize the total electric field energy. After the interface potentials are known, the coefficients of the above Fourier series are given by

$$A_n = \frac{4}{a_1 \sinh\left(\frac{n\pi h_1}{a_1}\right)} \int_0^{a_1/2} f(x) \cos\left(\frac{n\pi x}{a_1}\right) dx \tag{6a}$$

$$B_n = \frac{4}{a_2 \sinh\left(\frac{n\pi h_2}{a_2}\right)} \left[\cosh\left(\frac{n\pi h_2}{a_2}\right) \cdot \int_0^{s/2} g(x) \cos\left(\frac{n\pi x}{a_2}\right) dx - \cosh\left(\frac{n\pi (h_1 + h_2)}{a_2}\right) \int_0^{a_2/2} f(x) \cos\left(\frac{n\pi x}{a_2}\right) dx\right] \tag{6b}$$

$$C_n = \frac{4}{a_2 \sinh\left(\frac{n\pi h_2}{a_2}\right)} \cdot \left[\sinh\left(\frac{n\pi (h_1 + h_2)}{a_2}\right) \int_0^{a_2/2} f(x) \cos\left(\frac{n\pi x}{a_2}\right) dx - \sinh\left(\frac{n\pi (h_1 + h_2 + h_3)}{a_2}\right) \int_0^{s/2} g(x) \cos\left(\frac{n\pi x}{a_2}\right) dx\right] \tag{6c}$$

$$D_n = \frac{4}{a_3 \sinh\left(\frac{n\pi h_3}{a_3}\right)} \cdot \left[\cosh\left(\frac{n\pi (h_1 + h_2)}{a_3}\right) \int_0^{a_3/2} h(x) \cos\left(\frac{n\pi x}{a_3}\right) dx - \cosh\left(\frac{n\pi (h_1 + h_2 + h_3)}{a_3}\right) \int_0^{s/2} g(x) \cos\left(\frac{n\pi x}{a_3}\right) dx\right] \tag{6d}$$

$$E_n = \frac{4}{a_3 \sinh\left(\frac{n\pi h_3}{a_3}\right)} \cdot \left[\sinh\left(\frac{n\pi (h_1 + h_2 + h_3)}{a_3}\right) \int_0^{s/2} g(x) \cos\left(\frac{n\pi x}{a_3}\right) dx - \sinh\left(\frac{n\pi (h_1 + h_2)}{a_3}\right) \int_0^{a_3/2} h(x) \cos\left(\frac{n\pi x}{a_3}\right) dx\right] \tag{6e}$$

$$F_n = \frac{4}{a_4 \sinh\left(\frac{n\pi h_4}{a_4}\right)} \int_0^{a_4/2} h(x) \cos\left(\frac{n\pi x}{a_4}\right) dx. \tag{6f}$$

Now, the interface potentials can be conveniently expressed by spline functions, such as

$$f(x) = \sum_{i=0}^{m_1} F_i(x) \tag{7a}$$

$$g(x) = \sum_{i=0}^{m_2} G_i(x) \tag{7b}$$

$$h(x) = \sum_{i=0}^{m_3} H_i(x) \tag{7c}$$

where

$$F_i(x) = \begin{cases} \dfrac{p_i - p_{i+1}}{b_i - b_{i+1}}(x - b_{i+1}) + p_{i+1} & (b_i \leqslant x \leqslant b_{i+1}) \\ 0 & \text{(elsewhere)} \end{cases} \tag{8a}$$

$$G_i(x) = \begin{cases} \dfrac{q_i - q_{i+1}}{c_i - c_{i+1}}(x - c_{i+1}) + q_{i+1} & (c_i \leqslant x \leqslant c_{i+1}) \\ 0 & \text{(elsewhere)} \end{cases} \tag{8b}$$

$$H_i(x) = \begin{cases} \dfrac{r_i - r_{i+1}}{d_i - d_{i+1}}(x - d_{i+1}) + r_{i+1} & (d_i \leqslant x \leqslant d_{i+1}) \\ 0 & \text{(elsewhere)} \end{cases} \tag{8c}$$

and m_1, m_2, and m_3 are the numbers of knots at $y = h_1$, $y = h_1 + h_2$, and $y = h_1 + h_2 + h_3$, respectively.

When (4a), (4b), (4c), and (4d) are substituted into (2), the results of integration are expressed as

$$W = \sum_{j=0}^{m_1}\sum_{k=0}^{m_1} \zeta_{jk} p_j p_k + \sum_{j=0}^{m_2}\sum_{k=0}^{m_2} \eta_{jk} q_j q_k + \sum_{j=0}^{m_3}\sum_{k=0}^{m_3} \xi_{jk} r_j r_k + 2\sum_{j=0}^{m_1}\sum_{k=0}^{m_2} \mu_{jk} p_j q_k + 2\sum_{j=0}^{m_3}\sum_{k=0}^{m_2} \nu_{jk} r_j q_k \tag{9}$$

where ζ_{jk}, η_{jk}, ξ_{jk}, μ_{jk}, and ν_{jk} are given in Appendix I.

The total energy W is minimized by a differentiation procedure such as

$$\frac{\partial W}{\partial p_j} = 0 \qquad (j = 2,3,4,\cdots,m_1) \tag{10a}$$

$$\frac{\partial W}{\partial q_j} = 0 \qquad (j = 0,1,2,\cdots,m_2) \tag{10b}$$

$$\frac{\partial W}{\partial r_j} = 0 \qquad (j = 2,3,4,\cdots,m_3). \tag{10c}$$

The results of differentiation are given by a set of linear simultaneous equations as

$$\sum_{k=0}^{m_1} \zeta_{jk} p_k + \sum_{k=0}^{m_2} \mu_{jk} q_k = 0 \qquad (j = 2,3,4,\cdots,m_1) \tag{11a}$$

$$\sum_{k=0}^{m_1} \mu_{kj} p_k + \sum_{k=0}^{m_2} \eta_{jk} q_k + \sum_{k=0}^{m_3} \nu_{kj} r_k = 0 \qquad (j = 0,1,2,\cdots,m_2) \tag{11b}$$

$$\sum_{k=0}^{m_2} \nu_{jk} q_k + \sum_{k=0}^{m_3} \xi_{jk} r_k = 0 \qquad (j = 2,3,4,\cdots,m_3). \tag{11c}$$

Since the potentials of each conductor are known ($p_0 = p_1 = V_1$, $r_0 = r_1 = V_2$), these equations are rewritten as a set of inhomogeneous equations as

$$\sum_{k=2}^{m_1} \zeta_{jk} p_k + \sum_{k=0}^{m_2} \mu_{jk} q_k = -\sum_{k=0}^{1} \zeta_{jk} V_1 \qquad (j = 2,3,4,\cdots,m_1) \tag{12a}$$

$$\sum_{k=2}^{m_1} \mu_{kj} p_k + \sum_{k=0}^{m_2} \eta_{jk} q_k + \sum_{k=2}^{m_3} \nu_{kj} r_k = -\sum_{k=0}^{1} (\mu_{kj} V_1 + \nu_{kj} V_2) \qquad (j = 0,1,2,\cdots,m_2) \tag{12b}$$

$$\sum_{k=0}^{m_2} \nu_{jk} q_k + \sum_{k=2}^{m_3} \xi_{jk} r_k = -\sum_{k=0}^{1} \xi_{jk} V_2 \qquad (j = 2,3,4,\cdots,m_3). \tag{12c}$$

These linear equations can be easily solved on a computer. When the solutions of p_i, q_i, and r_i are substituted again into the energy expression (2), the value of W corresponds to $W_{\min}$.

Since the stored energy in this capacitor is $C_{11}V_1^2/2$, which should be equal to $W_{\min}$, C_{11} is given by

$$C_{11} = \frac{2W_{\min}}{V_1^2}. \tag{13}$$

When the conductor potentials are specified as $V_1 = 0$ and $V_2 \neq 0$, C_{22} can be calculated in a similar fashion. When the conductor potentials are specified as $V_1 = V_2 = V$, the capacitance $C = C_{11} + C_{22} + 2C_{12}$ can be calculated; C_{12} is then given by $(C - C_{11} - C_{22})/2$.

V. Numerical Processing and Accuracy

When the linear simultaneous equations (12a), (12b), and (12c) are solved as a matrix equation on a computer, it is important to reduce the size of the matrix and simplify the analytical expression of each element in order to reduce the computation time.

The size of the matrix is increased with the number of interface boundaries. When some geometrical symmetries exist in the structure, the size of the matrix can be effectively decreased. Since the structure in Fig. 2 is symmetrical, only half of the interface boundaries have to be considered. A typical number of spline knots was 16 for each interface in this case.

Secondly, the convergence of series appearing in matrix elements is considered. The series of μ_{kl} and ν_{kl} involving $\gamma_n(a_l, h_l) = 1/\sinh(n\pi h_l/a_l)$ converge fast because they behave as exponential functions. On the contrary, the series of ξ_{kl}, η_{kl}, and ζ_{kl} involving $\beta_n(a_l, h_l) = 1/\tanh(n\pi h_l/a_l)$ converge slowly and will always appear in the analyses of GSSL's. The convergence of such series can be improved by applying the summation formula discussed in Appendix II. As a result, the computation time for one value of capacitance was reduced to one-sixth the original time. A typical number of Fourier series terms in the present case was 160.

Since this method is based on the minimum-energy principle, the capacitance thus obtained is always larger than the true value. The accuracy of the calculated wavelength reduction factor and calculated characteristic impedance in a previous paper [3] were approximately 1 percent and 0.1 percent, respectively.

VI. Numerical and Experimental Results

The following parameters are taken for the purpose of comparison between theory and experiment:

$a_1 = 10$ $a_2 = 18$ $a_3 = 14$ $a_4 = 10$
$h_1 = 0.335$ $h_2 = 0.140$ $h_3 = 0.130$ $h_4 = 0.355$
$w_1 = w_2 = 5$ $S = 2 \sim 14$ (unit: mm)
$\epsilon_1 = \epsilon_4 = \epsilon_0$ $\epsilon_2 = \epsilon_3 = 2.22\epsilon_0$ (RT Duroid 5880).

Satisfactory convergence on capacitance values has been observed for the Fourier terms of 160 to 180 and for spline knot numbers greater than 16 for each boundary surface. The computation time for C_{11} was about 10 s on a HITAC M-260D computer and 1.5 min on a VAX 11/750 computer.

The line capacitance values were measured with a HP LCR meter by changing the length of the coupled lines. Fig. 4 shows reasonable agreement between calculated and measured capacitance values against the dimension of the aperture S. Since this structure is almost symmetrical, the coupling coefficient k is approximately defined by

$$k = \frac{Z_{\text{even}} - Z_{\text{odd}}}{Z_{\text{even}} + Z_{\text{odd}}} \tag{14}$$

where Z_{even} and Z_{odd} are the even-mode and the odd-mode impedance, respectively. Fig. 5 shows how the coupling coefficient k is controlled by the aperture dimension S.

VII. Another Example Structure

Fig. 6 shows another example of broadside coupled striplines. The thickness of strip and aperture conductors t_1, t_2, and t_3 are taken into account in this case. The analysis of capacitance matrix elements is carried out in a similar fashion to the preceding case except for the additional regions 1′, 3, and 5′. The derivation of analytical expressions is not included in this paper, however, since they can be straightforwardly processed.

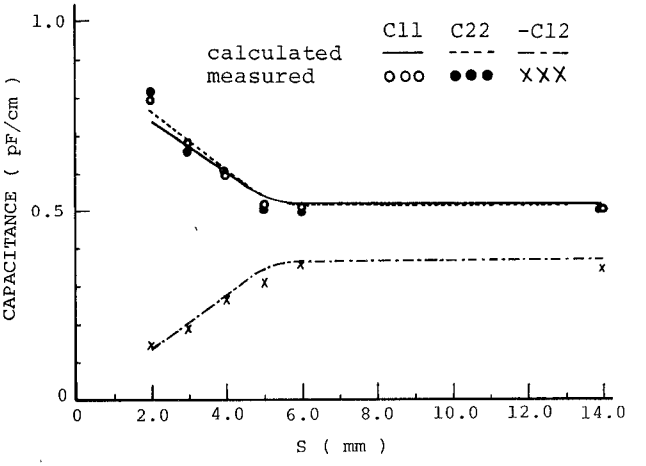

Fig. 4. Calculated and measured values of capacitance matrix elements.

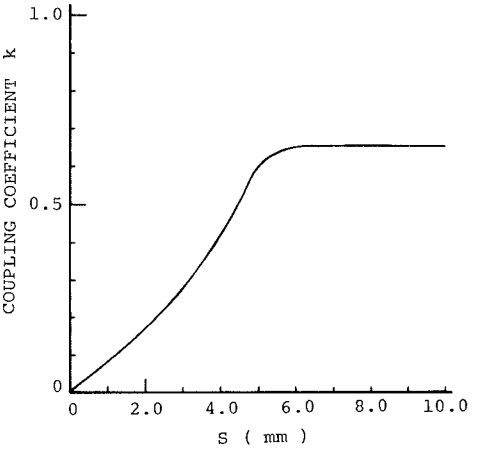

Fig. 5. Coupling coefficient values controlled by the dimension of the aperture.

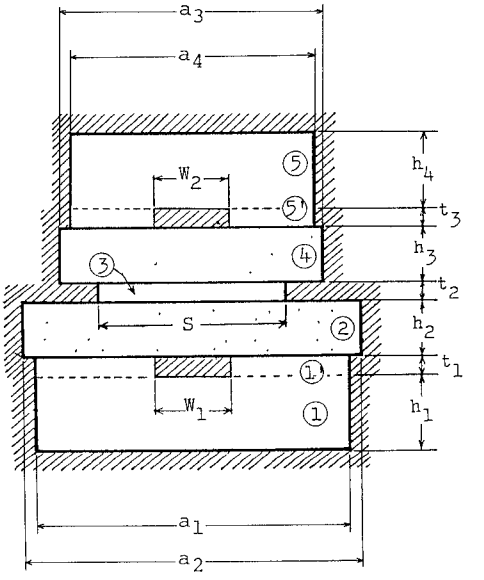

Fig. 6. Another example structure: A broadside coupled suspended thick stripline.

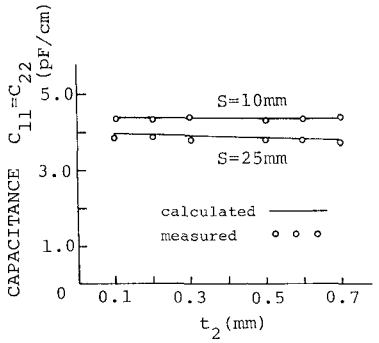

Fig. 7. Comparison of calculated and measured values of C_{11} for the structure of Fig. 6.

The parameters of this example are as follows:

$h_1 = h_4 = 0.5 \quad h_2 = h_3 = 2.0$
$a_1 = a_4 = 25.0 \quad a_2 = a_3 = 30.0$
$W_1 = W_2 = 16.0 \quad S = 10.0, 25.0$
$t_1 = t_3 = 0.035 \quad t_2 = 0.1 \sim 0.7$ (unit: mm)
$\epsilon_1 = \epsilon_{1'} = \epsilon_3 = \epsilon_5 = \epsilon_{5'} = \epsilon_0$
$\epsilon_2 = \epsilon_4 = 2.6\epsilon_0$ (Teflon composite material).

Theoretically calculated values of C_{11} are compared with measured ones in Fig. 7, which indicates good agreement. The computation time C_{11} in this case was about 4 min on a VAX 11/750 computer.

Appendix I

The parameters appearing in (12a), (12b), and (12c) are as follows:

$$\xi_{jk} = \sum_{n=1,3,5\cdots}^{\infty} \frac{2}{(n\pi)^3} \cdot \left[\epsilon_3 a_3^2 \beta_n(a_3, h_3)\alpha_n(a_3, d_j)\alpha_n(a_3, d_k) + \epsilon_4 a_4^2 \beta_n(a_4, h_4)\alpha_n(a_4, d_j)\alpha_n(a_4, d_k)\right] \quad \text{(A1)}$$

$$\eta_{jk} = \sum_{n=1,3,5\cdots}^{\infty} \frac{2}{(n\pi)^3} \cdot \left[\epsilon_2 a_2^2 \beta_n(a_2, h_2)\alpha_n(a_2, c_j)\alpha_n(a_2, c_k) + \epsilon_3 a_3^2 \beta_n(a_3, h_3)\alpha_n(a_3, c_j)\alpha_n(a_3, c_k)\right] \quad \text{(A2)}$$

$$\zeta_{jk} = \sum_{n=1,3,5\cdots}^{\infty} \frac{2}{(n\pi)^3} \left[\epsilon_1 a_1^2 (a_1, h_1)\alpha_n(a_1, b_j)\alpha_n(a_1, b_k) + \epsilon_2 a_2^2 \beta_n(a_2, h_2)\alpha_n(a_2, b_j)\alpha_n(a_2, b_k)\right] \quad \text{(A3)}$$

$$\mu_{jk} = \sum_{n=1,3,5\cdots}^{\infty} \frac{(-2)}{(n\pi)^3} \epsilon_2 a_2^2 \gamma_n(a_2, h_2)\alpha_n(a_2, b_j)\alpha_n(\alpha_2, c_k) \quad \text{(A4)}$$

$$\nu_{jk} = \sum_{n=1,3,5\cdots}^{\infty} \frac{(-2)}{(n\pi)^3} \epsilon_3 a_3^2 \gamma_n(a_3, h_3) \cdot \alpha_n(a_3, d_j)\alpha_n(a_3, c_k) \quad \text{(A5)}$$

$$\alpha_n(a_i, x_j) = \begin{cases} \dfrac{\cos\left(\dfrac{n\pi x_j}{a_i}\right) - \cos\left(\dfrac{n\pi x_{j-1}}{a_i}\right)}{x_j - x_{j-1}} - \dfrac{\cos\left(\dfrac{n\pi x_{j+1}}{a_i}\right) - \cos\left(\dfrac{n\pi x_j}{a_i}\right)}{x_{j+1} - x_j}, & j \geq 1 \\ \dfrac{1 - \cos\left(\dfrac{n\pi x_1}{a_i}\right)}{x_1}, & j = 0 \end{cases} \quad (i = 1,2,3,4) \quad \text{(A6)}$$

$$\beta_n(a_i, h_i) = \frac{1}{\tanh\left(\dfrac{n\pi h_i}{a_i}\right)} \quad (i = 1,2,3,4) \quad \text{(A7)}$$

$$\gamma_n(a_i, h_i) = \frac{1}{\sinh\left(\dfrac{n\pi h_i}{a_i}\right)} \quad (i = 1,2,3,4). \quad \text{(A8)}$$

Appendix II

The essential part of ξ_{jk}, η_{jk}, and ζ_{jk} in (9) is a series given by

$$\delta(a_i, h_i, x_j, x_k) \equiv \sum_{n=1,3,5\cdots}^{\infty} \frac{1}{n^3} \frac{1}{\tanh\left(\dfrac{n\pi h_i}{a_i}\right)} \cdot \alpha_n(a_i, x_j)\alpha_n(a_i, x_k) \quad (i = 1,2,3,4). \quad \text{(A9)}$$

Because $\alpha_n(a_i, x_j)\alpha_n(a_i, x_k)$ is a product of cosine functions, the series (A9) is eventually reduced to a linear combination of terms as

$$\delta_1(a_i, h_i, x_j) \equiv \sum_{n=1,3,5\cdots}^{\infty} \frac{1}{n^3} \frac{\cos\left(\frac{n\pi x_j}{a_i}\right)}{\tanh\left(\frac{n\pi h_i}{a_i}\right)} \quad \text{(A10)}$$

$$\delta_1(a_i, h_i, x_k) \equiv \sum_{n=1,3,5,\cdots}^{\infty} \frac{1}{n^3} \frac{\cos\left(\frac{n\pi x_k}{a_i}\right)}{\tanh\left(\frac{n\pi h_i}{a_i}\right)} \quad \text{(A11)}$$

which are rewritten as

$$\delta_1(a_i, h_i, x_j) = \sum_{n=1,3,5\cdots}^{\infty} \frac{1}{n^3} \left\{ \frac{1}{\tanh\left(\frac{n\pi h_i}{a_i}\right)} - 1 \right\} \cdot \cos\left(\frac{n\pi x_j}{a_i}\right) + \delta_0(a_i, x_j) \quad \text{(A12)}$$

where

$$\delta_0(a_i, x_j) \equiv \sum_{n=1,3,5,\cdots}^{\infty} \frac{\cos\left(\frac{n\pi x_j}{a_i}\right)}{n^3}. \quad \text{(A13)}$$

It is possible to sum $\delta_0(a_i, x_j)$ as

$$\delta_0(a_i, x_j) \cong \frac{7}{8} \sum_{n=1}^{\infty} \frac{1}{n^3} + \frac{\left(\frac{\pi x_j}{a_i}\right)^2}{4} \ln\left|\frac{\pi x_j}{a_i}\right| - \frac{3+2\ln 2}{8}\left(\frac{\pi x_j}{a_i}\right)^2 + \frac{1}{288}\left(\frac{\pi x_j}{a_i}\right)^4 + \frac{7}{86400}\left(\frac{\pi x_j}{a_i}\right)^6 + \cdots \qquad \left(-\pi < \frac{x_j}{a_i}\pi < \pi\right) \quad \text{(A14)}$$

where

$$\sum_{n=1}^{\infty} \frac{1}{n^3} = 1.2020569032\cdots. \quad \text{(A15)}$$

Since the first term on the right-hand side of (A11) is a rapidly converging series of exponential functions, the original series (A9) can also be changed to converge faster.

ACKNOWLEDGMENT

The authors thank their colleagues Dr. Y. Suzuki and A. Ohga for helpful suggestions in the process of programming.

REFERENCES

[1] C. I. Mobbs and J. D. Rhodes, "A generalized Chebyshev suspended substrate stripline bandpass filter," *IEEE Trans. Microwave Theory Tech.*, vol. MTT-31, pp. 397–402, May 1983.

[2] M. H. Arain, "A 94 GHz suspended stripline circulator," in *1984 IEEE MTT-S Int. Microwave Symp. Dig.*, pp. 78–79.

[3] E. Yamashita, B. Y. Wang, K. Atsuki, and K. R. Li, "Effects of side-wall grooves on transmission characteristics of suspended strip lines," in *1985 IEEE MTT-S Int. Microwave Symp. Dig.*, pp. 145–148; also *IEEE Trans. Microwave Theory Tech.*, vol MTT-33, pp. 1323–1328, Dec. 1985.

[4] R. E. Collin, *Field Theory of Guided Waves*. New York: McGraw-Hill, 1960, p. 148.

Eikichi Yamashita (M'66–SM'79–F'84) was born in Tokyo, Japan, on February 4, 1933. He received the B.S. degree from the University of Electro-Communications, Tokyo, Japan, and the M.S. and Ph.D. degrees from the University of Illinois, Urbana, all in electrical engineering, in 1956, 1963, and 1966, respectively.

From 1956 to 1964, he was a Member of the Research Staff on millimeter-wave engineering at the Electrotechnical Laboratory, Tokyo, Japan. While on leave from 1961 to 1963 and from 1964 to 1966, he studied solid-state devices in the millimeter-wave region at the Electro-Physics Laboratory, University of Illinois. From 1966 to 1967, he was with the Antenna Laboratory, University of Illinois. He became an Associate Professor in 1967, and Professor in 1977 in the Department of Applied Electronics, the University of Electro-Communications, Tokyo, Japan. His research work since 1956 has been on microstrip transmission lines, hybrid modes of Goubau lines, wave propagation in a gaseous plasma, pyroelectric-effect detectors in the submillimeter-wave region, tunnel-diode oscillators, wide-band laser modulators, and various types of optical fibers.

Dr. Yamashita is a member of the Institute of Electronics and Communication Engineers of Japan and of Sigma Xi. During the period 1980–1984, he served as an Associate Editor of the IEEE TRANSACTIONS ON MICROWAVE THEORY AND TECHNIQUES. He was elected Chairman of the Tokyo Chapter of the MTT Society for the period 1985–1986.

Masayuki Nakajima was born in Ibaraki, Japan, on July 8, 1958. He received the B.S. and M.S. degrees in electrical engineering from Sophia University, Tokyo, Japan, in 1982 and 1984, respectively.

He joined Tokyo Keiki Co., Ltd., Tokyo, Japan, in 1984. He studied analysis methods for microwave transmission lines as a visiting researcher at the University of Electro-Communications, Tokyo, Japan, in 1985.

Mr. Nakajima is a member of the Institute of Electronics and Communication Engineers of Japan.

Kazuhiko Atsuki was born in Tokyo, Japan, on November 2, 1942. He received the B.S. and M.S. degrees from the University of Electro-Communications, Tokyo, Japan, and the Dr. Eng. degree from Tokyo University, Tokyo, Japan, all in electrical engineering, in 1965, 1967, and 1979, respectively.

He became Research Assistant in 1967, Instructor in 1979, and Associate Professor in 1982 in the Department of Applied Electronics, University of Electro-Communications, Tokyo, Japan. He has been studying switching transistors, microstrip transmission lines, wide-band laser modulators, and optical fibers.

Dr. Atsuki is a member of the Institute of Electronics and Communication Engineers of Japan.